

Recent results from the Pierre Auger Observatory

James W. Cronin
for the Auger collaboration

*Department of Astronomy and Astrophysics
Enrico Fermi Institute, University of Chicago
5640 South Ellis Ave. , Chicago, IL 60637, USA*



We report on the observations of cosmic rays with energies $\geq 10^{18}$ eV from Jan 2004 to April 2009 by the Pierre Auger Observatory. During this period the Observatory has grown from about 300 surface detectors to about 1600 upon its completion in November 2008. The 1600 surface detectors are overlooked by 24 fluorescence telescopes. We report on measurements of the cosmic ray spectrum, the arrival directions and the elongation rate. We also report limits for the photon and neutrino components of this cosmic radiation.

1 Introduction

The cosmic radiation discovered by Hess¹ extends from very low energies $\leq 10^6$ eV to $\geq 10^{20}$ eV. The latter energy is equal to 16 joules - a macroscopic energy in a microscopic particle as the cosmic rays are principally atomic nuclei ranging from protons to iron. Figure 1 shows the full cosmic ray spectrum. It is roughly a power law falling by 30 orders of magnitude in flux over 10 orders of magnitude increase in energy. The upper end of the spectrum represents a mystery as there is no clear understanding of how Nature can accelerate atomic nuclei to such high energies. The study of this category of cosmic rays is a scientific imperative and Nature provides two important analytical tools for the investigation.

First, the very highest energy cosmic rays must come from nearby. Consequently one can expect that there are a small number of sources that can contribute to the flux of the highest energy cosmic rays. Protons interact with the cosmic microwave background (CMB) losing energy while producing pions. This is the famous GZK effect. Complex nuclei are photo disintegrated by the CMB. The result of these interactions is that half of the cosmic rays with energy $\geq 6 \times 10^{19}$ eV must come from distances less than 70 Mpc². In Figure 2 we show the expected distribution of distances for several nuclear species on the basis of a uniform source distribution. It is noteworthy that for distances ≥ 50 Mpc only protons and iron nuclei survive. In composition analysis at these high energies the assumption of two components is more than just an ansatz - it is a reasonable assumption.

Second, the higher energies and shorter distances will reduce the effects of the random magnetic fields which at lower energies decouple the observed arrival direction from the true

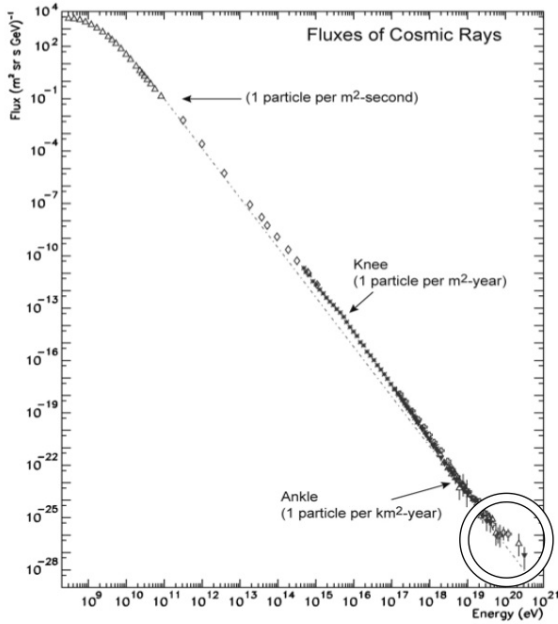


Figure 1: *Cosmic ray spectrum (data compiled by Simon Swordy, University of Chicago).*

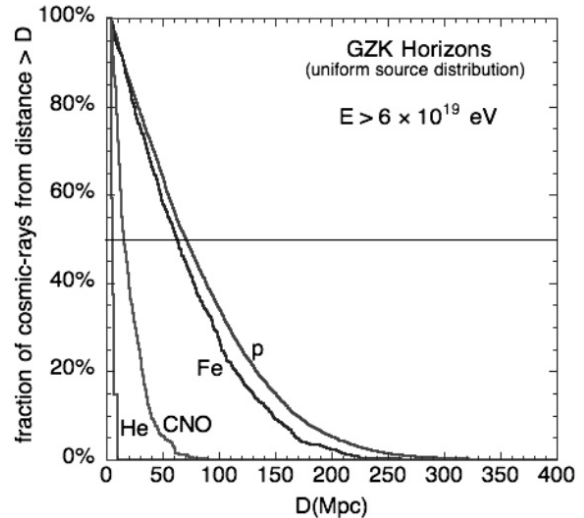


Figure 2: *GZK horizons for protons and nuclei (figure courtesy Denis Allard).*

direction of the source.

Thus it is quite possible that the arrival directions for energies $\geq 6 \times 10^{19}$ will correlate with the distribution of extragalactic objects located within 100 Mpc.

2 Techniques for measurement of the highest energy cosmic rays

Cosmic rays with energies above 10^{15} eV are detected by the shower of particles they produce in the atmosphere. The flux is too small for direct detection. There are two basic means to detect these showers: either by detecting the particles on the ground or by detecting the nitrogen fluorescence produced by the charged particles in the atmosphere. In Figure 3 we show a cartoon which illustrates the two techniques.

The fluorescence technique measures the energy dissipated in the atmosphere by the electromagnetic shower particles. Absolute calibration of the detector is required, details of atmospheric absorption must be independently measured and the absolute fluorescence yield must be known. In principle these requirements can be achieved. The disadvantage of the fluorescence technique is that its duty cycle is about 10% as fluorescence can only be observed on dark moonless nights.

Detection on the ground has a 100 % duty cycle but relating the cosmic ray energy to the observed ground signals requires simulation of hadron induced showers where the details of the first interactions are at energies well beyond laboratory observations.

Prior to the Auger Observatory there have been two very large detectors which have measured the cosmic ray spectrum at the highest energy. One, HiRes³, used the fluorescence technique, the other, AGASA⁴ detected the ground particles. At the highest energies as shown in Figure 4 the spectra of the two detectors disagree. HiRes shows a steepening of the spectrum as expected from the GZK effect while AGASA showed a continuation of the spectrum. This latter spectrum was the subject of extensive speculation about possible exotic sources of cosmic rays.

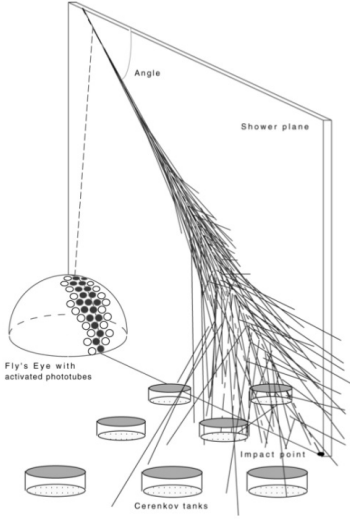


Figure 3: *Cartoon showing the two techniques for detection of air showers (figure courtesy Enrique Zas .*

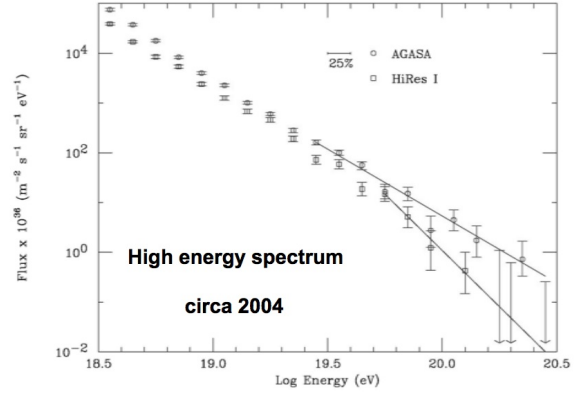


Figure 4: *Cosmic ray spectra from HiRes and AGASA circa 2004 .*

3 The Pierre Auger Observatory

The Pierre Auger Observatory has been built by an international collaboration of 17 countries. It was conceived in 1992 and designed in 1995. The design combines a surface detector (SD) with a fluorescence detector (FD). This hybrid design permits very accurate reconstruction of the shower geometry if a single tank is triggered in coincidence with a fluorescence event. The hybrid reconstruction is more precise than in the case for a shower seen in stereo by two fluorescence telescopes. SD events that reconstruct and have a coincident fluorescence reconstruction are called golden hybrid events. These golden hybrid events are used to calibrate the surface detector which operates with a duty cycle close to 100 %.

The site in Malargüe, Mendoza Province, Argentina was dedicated in 1999. Construction began in 2000. Data taking began Jan 1 2004 and the observatory was completed in Nov 2008. The location is shown in Figure 5. Figure 6 shows the configuration of the observatory. There are 1600 water Cerenkov detectors surrounded by four buildings each containing 6 fluorescence telescopes. Each telescope has a view of 30° in azimuth and 30° in elevation. A view of a fluorescence building and a Cerenkov tank is shown in Figure 7. The tanks communicate with a central station by radio and microwaves. The power for the tank electronics is provided by solar panels. The time of the tank signal is measured by a GPS unit. A technical description of the observatory has been published⁵.

Each Cerenkov tank is 3.5 m in diameter, 1.2 m high and contains 12 tons of purified water. It is lined with a diffuse reflector and is viewed by three 9-inch PMT's. In Figure 8 we show part of the event display. The upper left panel shows the fitted lateral distribution of a large shower corresponding to an energy 7.5×10^{19} eV. The upper right panel shows the strength of the signals in the triggered tanks. The magnitude of the signal in each tank is measured in "vertical equivalent muons" (VEM), a quantity easily inferred by the abundant single muons passing through each tank. The zenith angle is 34° . Showers with zenith angles $\leq 60^\circ$ are classified as "young" showers - showers initiated close to the ground. A characteristic of the "young" showers is the large spread in time of arrival of the shower particles as shown in the panel on the lower right. These particles are dominated by the electromagnetic component of the shower. "Young" showers are easily reconstructed and make up the sample for most of the results reported here. The signal at 1000 meters is the energy parameter of the shower which is



Figure 5: *Location of Pierre Auger Observatory in Argentina.*

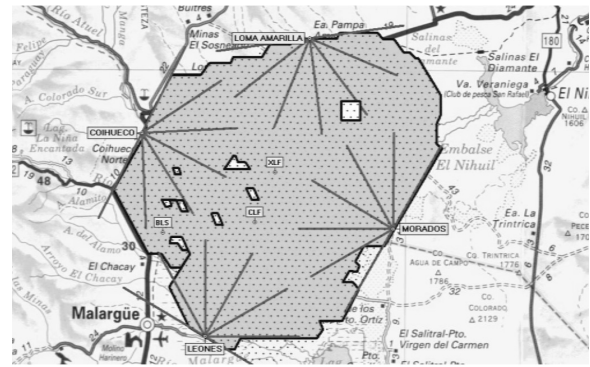


Figure 6: *Layout of Pierre Auger Observatory as of July 2009 .*

calibrated by the fluorescence detector.



Figure 7: *View of Cerenkov tank with fluorescence telescope building in the background.*

Showers with large zenith angles are easily detected. In Figure 9 we show parts of the event display for a shower with a zenith angle of 72° . These are classified as “old” showers as they are initiated far from the ground. They are distinctively different from the “young” showers. The time of arrival distribution shown in the lower right panel is very narrow. This is because the electromagnetic part of the shower has been absorbed and only the muons remain. The muons travel essentially un-deflected at the speed of light. Were one to observe a shower at a large zenith angle with a large spread in arrival times it would have had to be initiated deep in the atmosphere. Such a shower would be evidence for a weakly interacting particle - a neutrino.

In Figure 10 we show two views of one of the fluorescence telescopes. On the left the mirror and rear of the camera is shown. The mirror is spherical. Schmidt optics is used. On the right the entrance window with the Schmidt corrector and the face of the camera is shown. The window is a filter which transmits only the near ultra-violet fluorescence light. In Figure 11 we show the

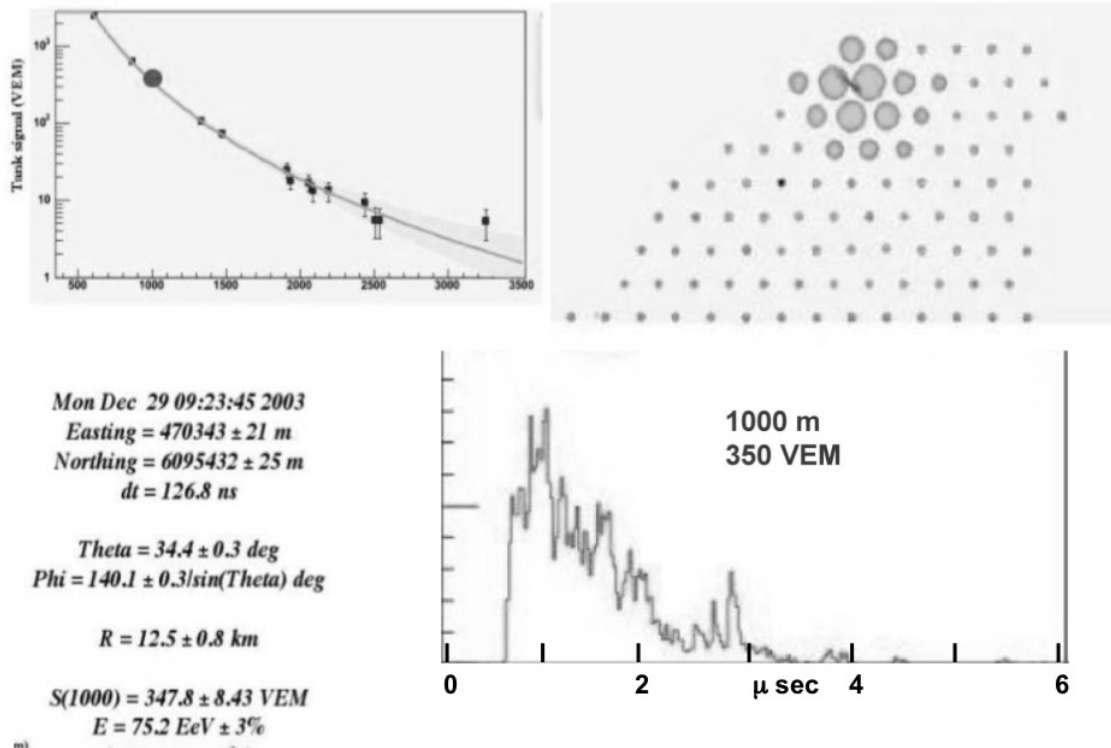


Figure 8: Portion of event display for a "young" shower.

display of a particularly beautiful hybrid event. The upper left is the image of the shower on the camera face. Upper right is the angle of the received light plotted against the time of arrival of the light. The dark points are the times observed with the fluorescence telescope and the lighter points are the times derived from the coincident tanks. An accurate geometrical measurement requires a determination of the curvature in this plot. The additional points provided by the surface detector greatly improve the curvature measurement. The panel on the lower left shows the pattern of triggered tanks on the surface. The panel on the lower right shows the longitudinal profile of the shower. The integral of this curve gives the electromagnetic shower energy. Muons and neutrinos are also present in the showers and carry additional energy which must be added to the electromagnetic energy. This energy is model dependent and comprises about 7 to 14 % of the electromagnetic energy. An additional 10 % is added to the energy along with a 5% systematic error.

4 The cosmic ray spectrum

The surface array of the Pierre Auger observatory is calibrated by the fluorescence detector. The intensities of the fluorescence lines and their pressure dependence have been measured relative to the 337 nm line⁶. The yield of the 337 nm line is taken to be 5.05 photons / MeV⁷. The energy parameter for the surface array is the signal in VEM measured at 1000 m from the reconstructed core. For a fixed energy this quantity varies with the zenith angle of the shower. The effective attenuation can be determined from the data assuming that the intensity of cosmic rays for a fixed energy must be independent of the zenith angle. This *Constant Integral Intensity* method was pioneered by the MIT group⁸. The signal that each shower produces at 1000 m is adjusted to the signal that would have been produced at a zenith angle of 38⁰. This is the median angle

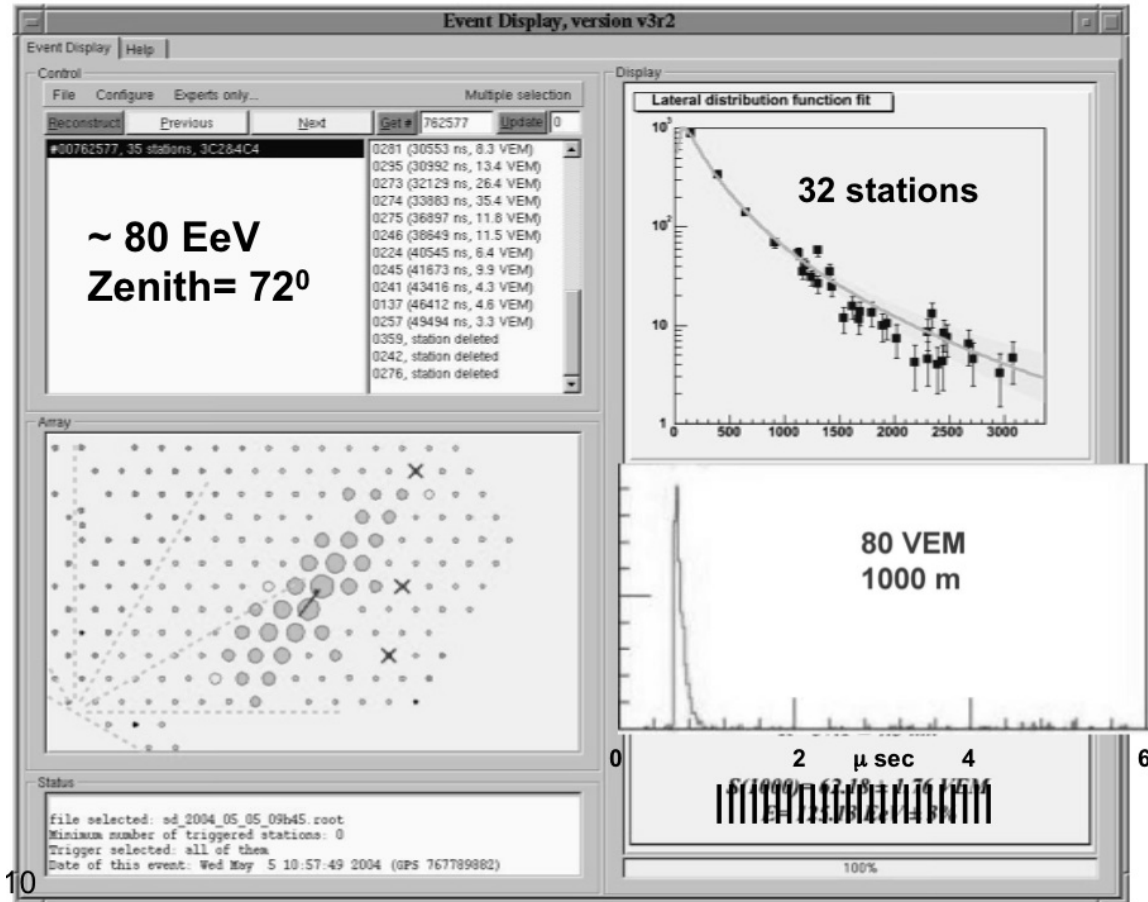


Figure 9: Portion of event display for an inclined shower.

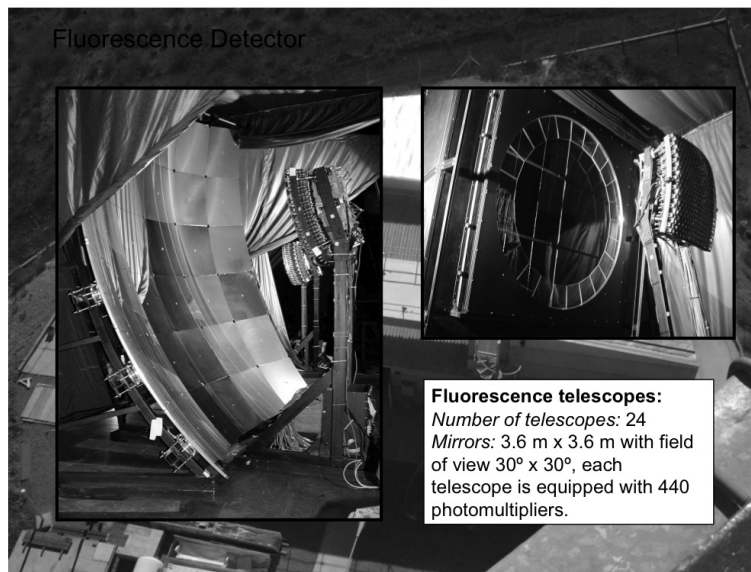


Figure 10: Two views of a fluorescence telescope.

for the cosmic ray sample with zenith angle $\leq 60^\circ$. In Figure 12 we plot this signal called S_{38} vs the energy determined by the fluorescence telescopes. The correlation is excellent. The

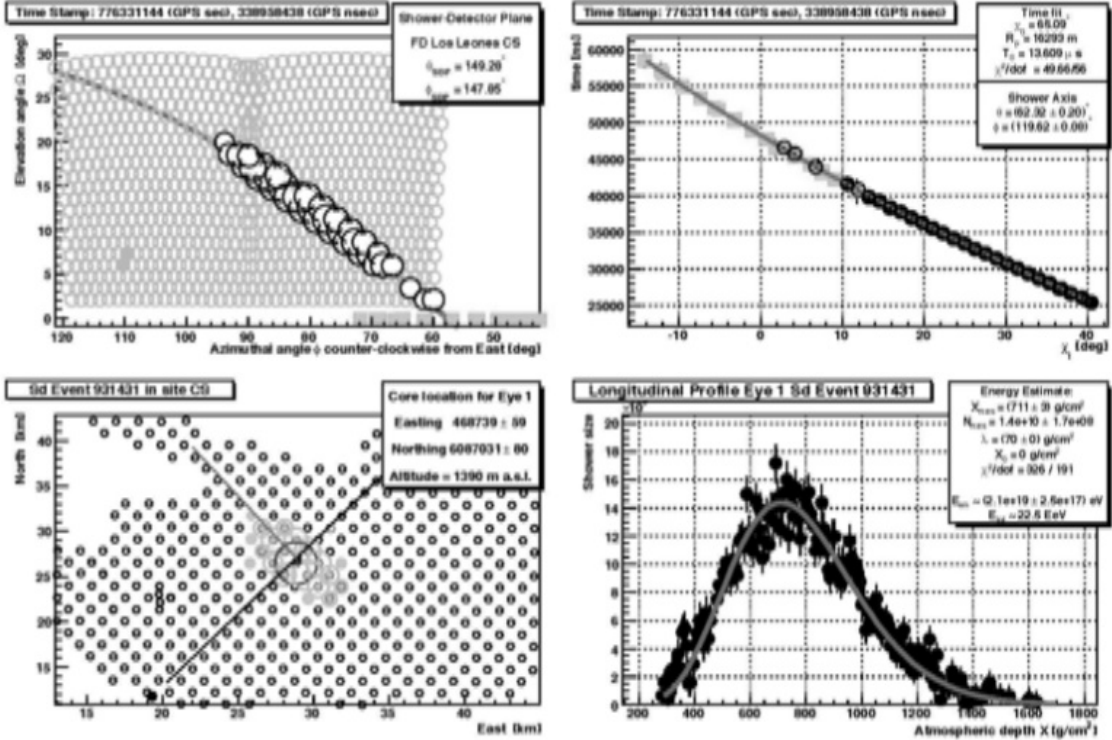


Figure 11: *Event display for an hybrid event.*

inset shows the distribution of the fractional difference between the fluorescence energy and the surface energy determined by the calibration curve of Figure 12. The width of 20% shows the statistical fluctuations in the energy determination of the surface events. The systematic error in the energy determination is estimated to be 22%.

In Figure 13 we show the spectrum as reported at the 2007 ICRC⁹. This spectrum is a composite of the spectra measured by the surface detector, by hybrid events, and by inclined showers. The spectrum from the surface detector alone was published in 2008¹⁰. In Figure 14 we plot the number of events recorded up to April 6, 2009 vs energy. This curve is an unnormalized energy spectrum as the surface array is fully efficient for energies above 3×10^{18} eV and is more than 80 % efficient at 10^{18} eV. By eye one can see the steepening of the spectrum above $10^{19.5}$ eV and the ankle at about $10^{18.5}$ eV. The falloff at $10^{19.5}$ eV is consistent with the GZK cutoff but not a proof of its observation. A discussion of the significance of these features was presented in the parallel sessions by Victor Olmos-Gilbaja¹¹.

5 The high energy sky

In the November 9, 2007 issue of Science Magazine¹² the Auger collaboration published a correlation of events with energies ≥ 55 EeV with the Véron-Cetty catalog of AGN's¹³. For the first 15 events a scan was made searching for the best correlation with the catalog. The scan was made over angular distance of the observed to the catalog events, the minimum energy of the observed events and the red shift of the catalog events. The maximum correlation was found for an angle of 3.1° , a red shift of ≤ 0.018 (75Mpc), and an energy ≥ 55 EeV. A test with the next 12 events confirmed this correlation with a 99% confidence level. A plot of the arrival directions for these 27 events is shown in Figure 15. The circles of 3.1° indicate the location of the cosmic ray events. The points are the direction of the objects in the catalog. Nineteen of

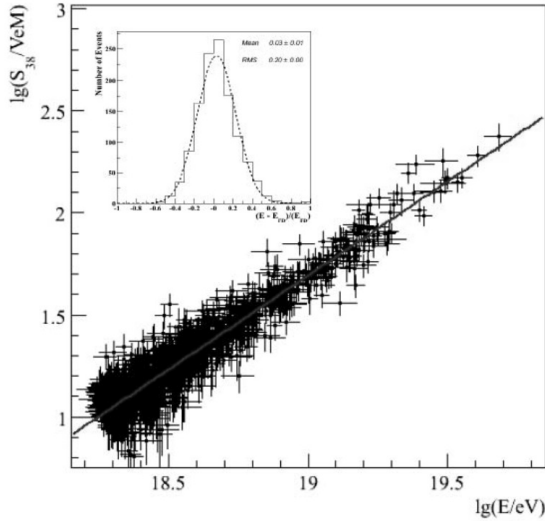


Figure 12: Plot of the energy parameter S_{38} vs the energy determined by the fluorescence telescopes.

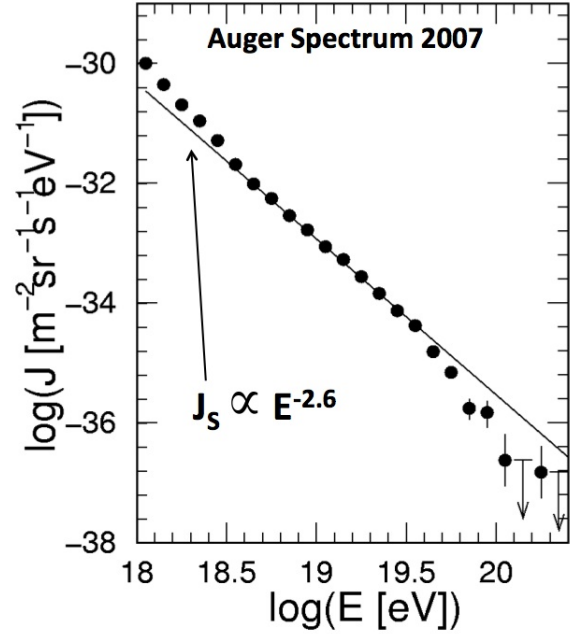


Figure 13: Plot of the number of SD events with zenith angle $\leq 60^\circ$ vs energy through April 4, 2009).

the 27 events correlate with the catalog.

The scan in energy, red shift, and correlation angle was made with no explicit assumption of anisotropy. One can ask the question: “Is the distribution in the sky of the arrival directions of the events with energy ≥ 55 EeV consistent with an isotropic one?” Note that 55 EeV is the energy for which the event rate is reduced by about a factor of 2 from the rate extrapolated from the slope fitted between $10^{18.6}$ to $10^{19.4}$ as shown in Figure 14. If the fall off is the GZK feature one may expect an onset of anisotropy at and above that energy as the horizon for possible sources is significantly reduced. A test for isotropy was developed in May 2007. This test has been applied without alteration to all the events with energy ≥ 55 EeV as they have accumulated. The details of the isotropy test are given in the Appendix.

In Figure 16 we plot the isotropic probabilities for the events observed up to August 31, 2007 as a function of their energy range. Each point corresponds to a group of 27 events. The highest energy point is the isotropic probability for the events with energy ≥ 55 EeV. The remaining points are the isotropic probabilities for 27 events at successively lower energies. The conclusion from this plot is that a significant anisotropy exists only in the highest energy bin. All lower energy bins are consistent with isotropy. This observation is what one expects from the GZK effect - only the highest energy bin contains events that are enhanced from sources nearby where the distribution of extra-galactic sources is known to be anisotropic.

We have made the identical analysis as further events have been accumulated. In Figure 17 we plot the time of arrival of these energetic events as a function of time. As of April 4, 2009 58 such events have occurred. Also plotted is the number of these events which fall within 3.1° of the objects of the Véron-Cetty catalog with red shift ≤ 0.018 . The smooth curve shows the accumulation of the relative exposure. The vertical line marks the situation on August 31, 2007. One can see that the rate of accumulation of the correlating events slowed significantly after August 31. In Figure 18 we repeat the probability of isotropy as a function of energy in groups of 58 events. The conclusion that only the highest energy bin is anisotropic remains.

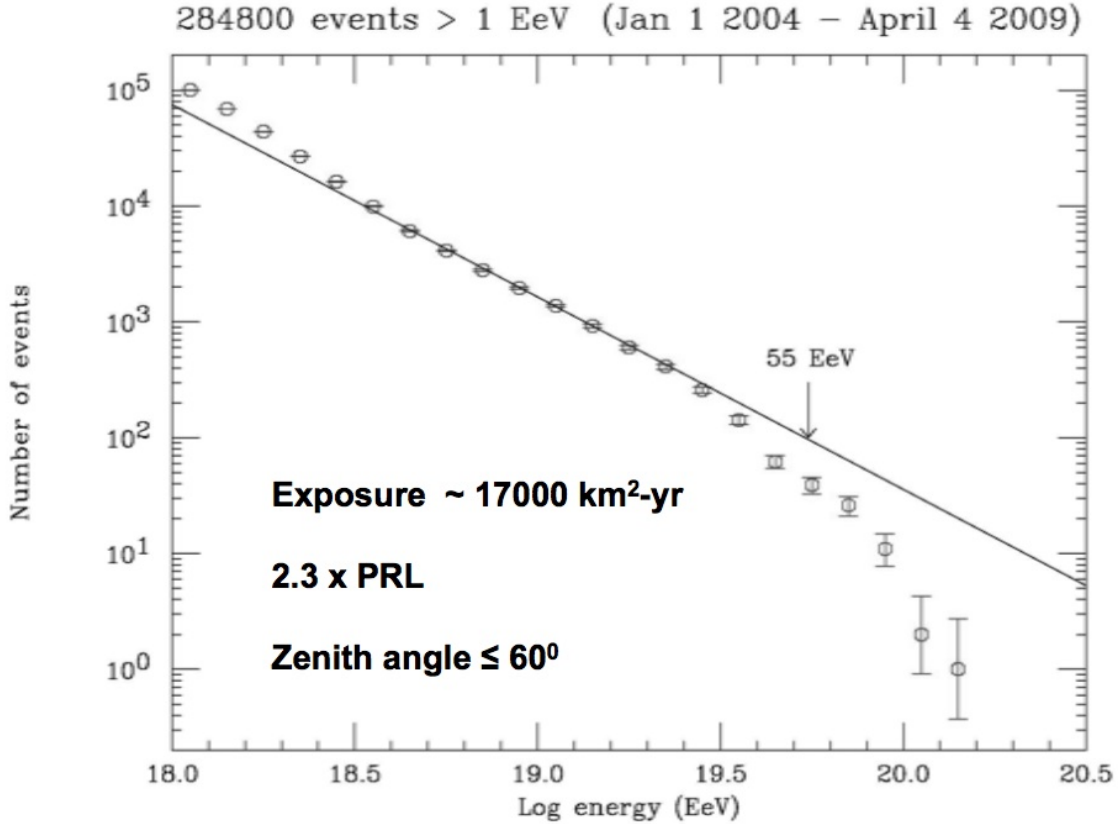


Figure 14: Plot of the number of SD events with zenith angle $\leq 60^\circ$ vs energy through April 4, 2009.

The isotropic probability for that bin is larger but the result is still significant and the basic conclusion - anisotropy is observed only in the highest energy bin - remains. We emphasize once more that the onset of the anisotropy coincides with the fall off of the spectrum. This evidence is consistent with the interpretation of the primaries as protons. Naively one would not expect a significant anisotropy if the primaries were iron nuclei.

A more detailed discussion of the high energy sky was presented in a parallel session by Carla Bonafazi¹⁴.

6 Elongation rate

The longitudinal development of the electromagnetic part of the shower is directly measured by the fluorescence telescopes. Figure 19 shows qualitatively how the shower maximum depends on the nature of the primary. The upper curve is a plot of the mean depth in the atmosphere of the shower maximum for a photon primary. The maximum is a linear function of the logarithm of the primary energy with a slope of about $80 \text{ gm/cm}^2/\text{decade}$. This slope is called the elongation rate. (This curve is modified above an energy $10^{19.5} \text{ eV}$ by the LPM effect and early conversion in the earth's magnetic field, but those complications do not alter the discussion here.) The middle curve shows the mean shower maximum vs energy for a proton primary. The exact location of this curve on the plot depends on the particular hadronic interaction model used for its calculation. However the elongation rate is much less sensitive to the model and is typically $50 \text{ gm/cm}^2/\text{decade}$ for a single nuclear species. The lower curve is the same quantity for iron primaries. The mean shower maximum for iron nuclei is about 100 gm/cm^2 less deep in the

27 events: energy > 55 EeV (Jan 1 2004 to Aug 31 2007)

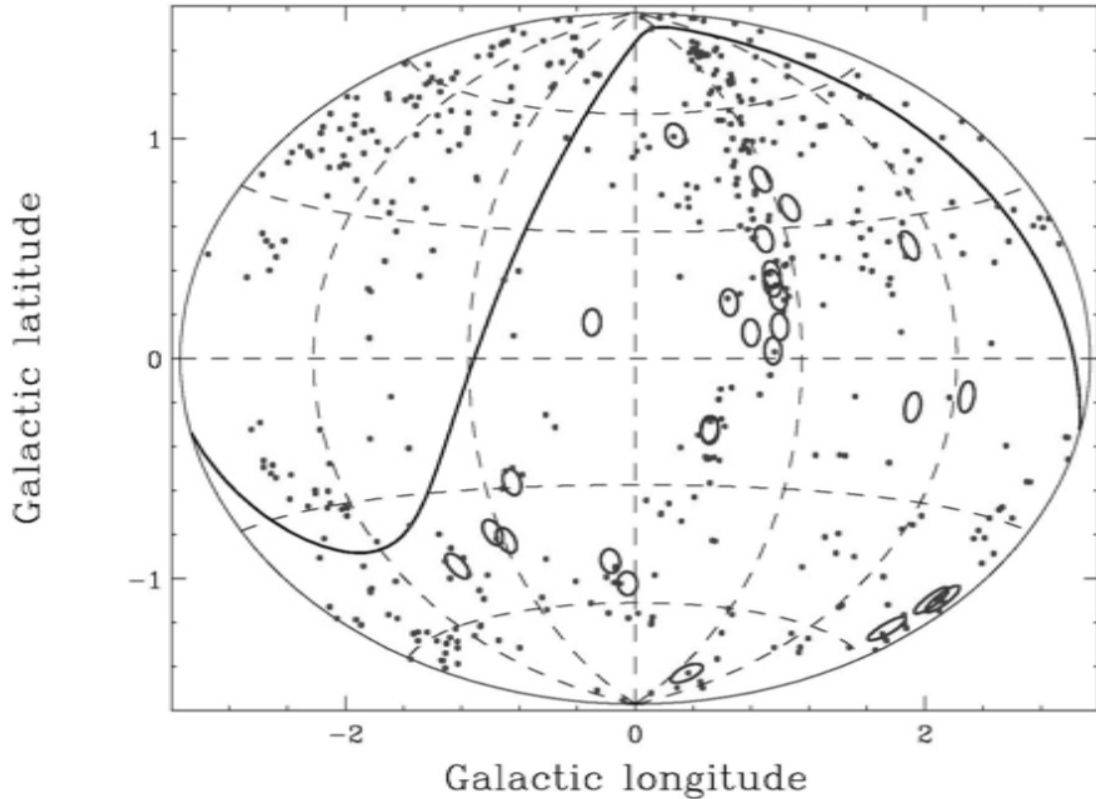


Figure 15: *Distribution of arrival directions for 27 events with energy ≥ 55 EeV observed through Aug 31, 2007. The events are represented by circles of 3.1° . The points are 472 objects the Véron-Cetty catalog (see text).*

atmosphere than for protons of the same energy and the elongation rate is nearly identical with a proton primary. This relation is nearly independent of the particular hadronic interaction model.

The fluctuation of the shower maximum about its mean depends strongly on the mass of the primary. Roughly the depth of a given shower maximum reflects the depth of the first interaction. The fluctuation of the shower maximum for a proton primary will be much greater than for an iron primary because the interaction cross section for a proton is much less than for an iron nucleus. The fluctuation for a proton is expected to be about 60 gm/cm^2 while for iron it is expected to be about 25 gm/cm^2 .

Figure 20 shows the measured quantities. On the left panel is the mean value of the shower maximum. The highest energy point is centered on $10^{19.5}$ eV (31 EeV) which does not overlap the energy, 55 EeV where the onset of the anisotropy occurs. This lack of overlap is due to the fact that the duty cycle for fluorescence events is only 10%. But there are significant trends which likely will extend to the highest energies observed. A constant composition as the energy increases would give a constant elongation rate of about $50 \text{ gm/cm}^2/\text{decade}$. The data show a larger elongation rate below $10^{18.5}$ and a smaller elongation rate above. This would suggest the composition becoming lighter below $10^{18.5}$ and becoming heavier above. On the right panel is a more dramatic picture - the RMS changing from a value roughly consistent with light (proton) primaries to values consistent with heavy (iron) primaries.

Figure 21 shows the data with the addition of the predictions for four different interaction models. The qualitative conclusions drawn above are not altered. If these trends persist to the highest energies there would appear to be a conflict between conclusions that can be drawn from

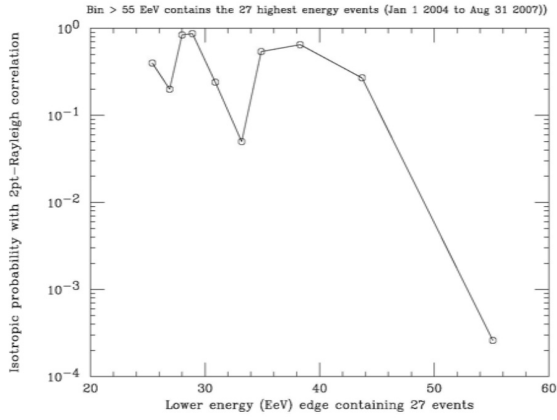


Figure 16: Plot of isotropic probability as function of energy (see text).

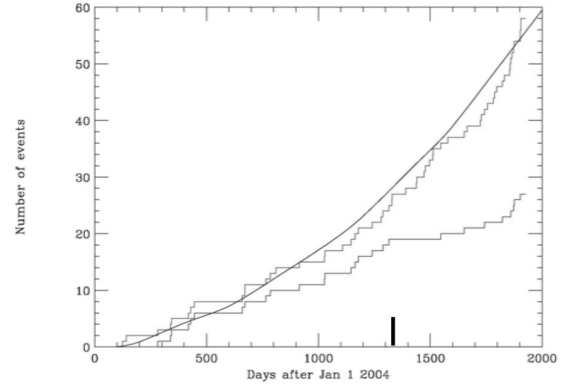


Figure 17: Upper histogram: cumulative highest energy events vs time. Lower histogram: cumulative events that correlate with the Véron-Cetty catalog. Smooth curve: cumulative relative aperture.

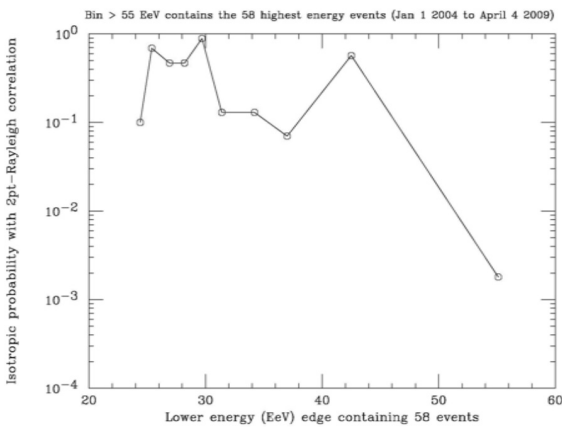


Figure 18: Plot of isotropic probability as function of energy for events recorded through April 4, 2009.

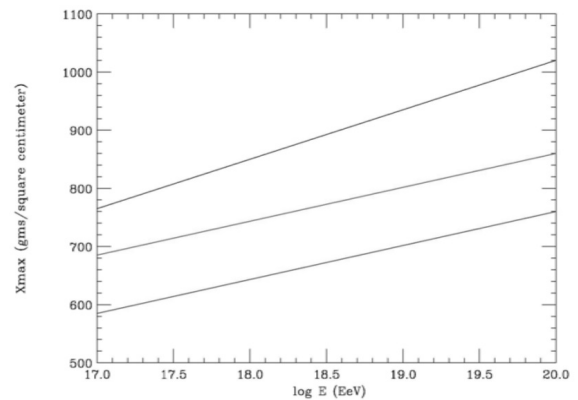


Figure 19: Elongation rates for photons, protons, and iron nuclei. (see text).

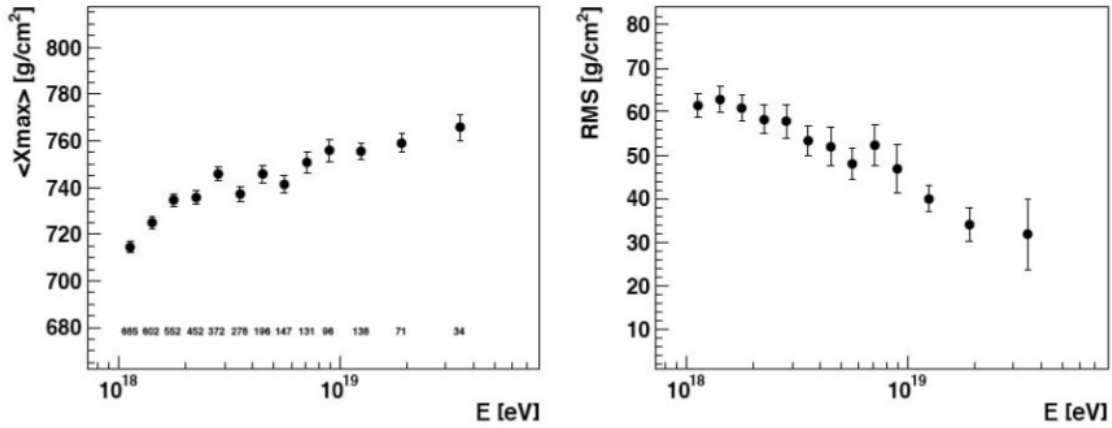


Figure 20: *Left panel: Measured mean depth of shower maximum vs energy. Right panel: Measured RMS for the depth of shower maximum vs energy.*

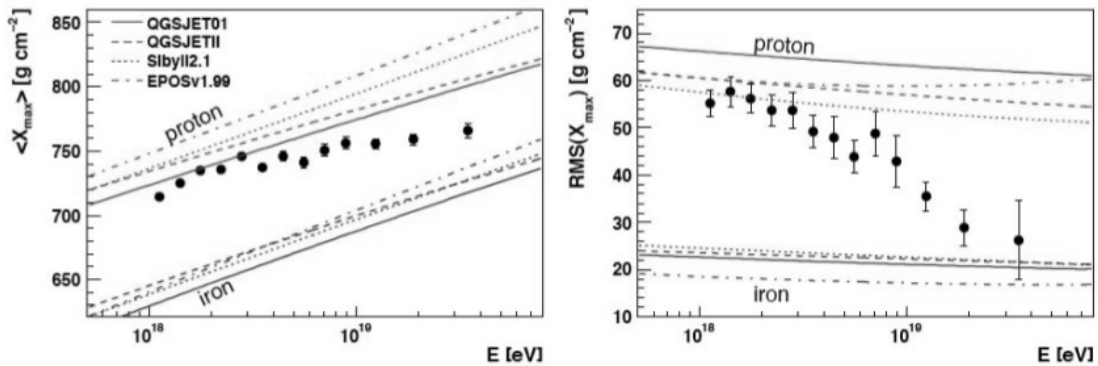


Figure 21: *Same as Figure 20 with the addition of predictions of various hadronic interactional models.*

the anisotropy and the conclusions drawn from the elongation rate measurement. Needless to say the elongation rate measurement came as a complete surprise. I suspect that only a small number of astrophysicists would have predicted that at the highest energies the composition would be rich in iron nuclei. This unexpected result has had extreme scrutiny within our collaboration. These results also demand a more careful review of what seemed to be an obvious conclusion that iron nuclei could not show an anisotropy because of galactic and perhaps extragalactic magnetic fields.

It is natural to say we need more data. The present data sample represents about 3 years of operation of the completed array. Another 3 years will only double the sample. The rate of the GZK sensitive events is only 20/year so we do not expect any significant change in the nature of the anisotropy that might bear on the question of composition. The proposed northern observatory in south eastern Colorado will have seven times the sensitivity. It is likely that this array will be required to resolve some of the scientific issues raised by the southern observatory.

A presentation of the details of the elongation measurement has been presented in a parallel session by Victor de Souza¹⁵

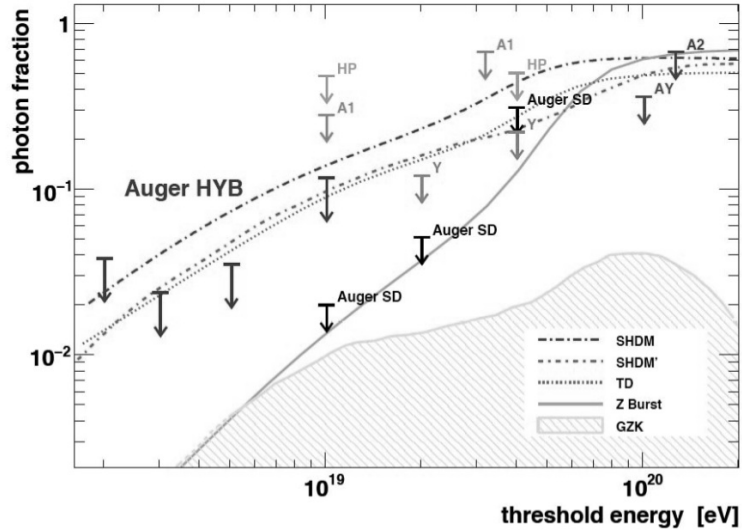


Figure 22: Summary of limits to the photon fraction in cosmic rays as a function of energy.

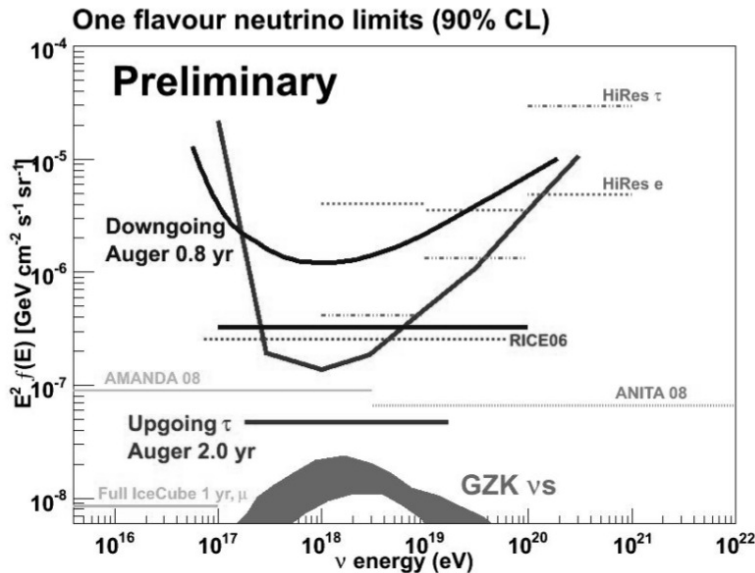


Figure 23: Summary of limits to the neutrino flux.

7 Photon limits

There have been several analyses of the photon fraction contained in the highest energy cosmic rays. No photons have been observed. The 90% confidence upper limits are summarized in Figure 22. The result is that the fraction of primary photons is $\leq 2\%$ above 10^{19} eV and $\leq 10\%$ at $10^{19.5}$ eV. This result rules out a number of exotic sources proposed to explain the highest energy cosmic rays. Note that at the very highest energy, while no photon has been observed the limits are not stringent because of lack of events of any kind. A presentation of the details of the photon limits has been presented in a parallel session by Mariangela Settimo¹⁶.

8 Neutrino limits

As was mentioned above, a highly inclined shower which has the character of a young shower is the signature of a neutrino. A shower with similar properties is also produced when a tau lepton decays just above the array. The latter showers can be produced by tau neutrinos skimming the earth. A tau lepton produced in the earth, emerges and decays. A search has been made for such young inclined showers and no candidates have been found. In Figure 23 we plot the corresponding limits for each process. Shown in the plot are the differential limits and the corresponding integral limits assuming a flux that falls as E^{-2} . The Auger observatory is most sensitive to neutrinos resulting from interactions of cosmic ray protons with the CMB. It is just possible that in the lifetime of the observatory a few neutrinos will be seen. We should point out here that if the highest energy cosmic rays are heavy nuclei the estimate of the neutrino flux from CMB interactions will be much less than the indicated prediction. A presentation of the neutrino limits has been presented in a parallel session by Sergio Navas¹⁷.

9 Conclusions

I have tried to cover the principal results that the observatory has produced so far. There are many detailed analyses that concern and question the hadronic models that are used in parts of the analysis. Discussion of these analyses is beyond the scope of this talk and perhaps even the scope of the author. I have stressed those results that are not strongly dependent on the models. The fact that one can make the energy calibration largely independent of the hadronic models is a strong point of the experiment. But the tension between the anisotropy and the elongation rate is something totally unexpected and yet to be resolved. The reliability of the array is continuously being improved. Additions of auxiliary equipment will extend the reach of the observatory particularly to lower energies so one will have a sweep in energy of more than three orders of magnitude from $\leq 10^{17}$ eV to beyond 10^{20} eV. Development of a possible new detection technique, radio, is actively being pursued at the site.

Acknowledgments

The author wants to thank his many colleagues who have aided in his understanding of all the physics involved in cosmic rays. These colleagues are far too numerous to mention individually. He wants to thank those unmentioned colleagues who have encouraged some of his unconventional observations about the data, particularly with respect to the high energy sky. Finally the observatory would never have become a reality without the dedication of Paul Mantsch who managed and directed the construction of the Observatory. And last but not least this author has been overwhelmed by the originality of all the data analyses done in large part by creative young men and women from all parts of the globe.

Appendix

In April 2007 as the evidence for the correlation of the highest energy events with astrophysical catalogs was developing, I and my colleagues at the University of Chicago thought it important to ask the question: Is there an anisotropy in the data independent of any reference to a catalog of sources? Scans of the data had identified a minimum energy for the strongest correlation, 55EeV. I made a distribution of all the angular distances between all pairs of events. This distribution was not consistent with an isotropic distribution. My colleagues, principally Maximo Ave and Lorenzo Cazon added a "Rayleigh-like" test. We named this the 2pt-Rayleigh test. I have applied this test for isotropy of the data for the last two years as the sample increased from the

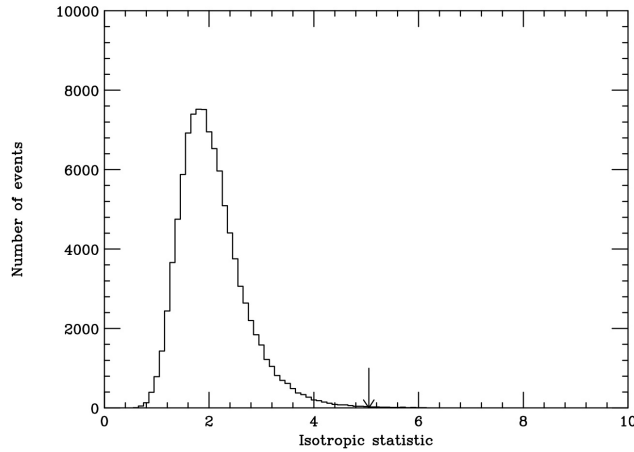


Figure 24: *Distribution of the 2pt-Rayleigh statistic for 58 events drawn from an isotropic distribution. Arrow shows value of the statistic for the data*

27 events ≥ 55 EeV on August 31, 2007 to the 58 discussed in this talk. An evaluation of these class of tests is given in reference 18.

The test proceeds as follows: All possible angular differences between pairs of events are divided into 14 angular intervals of 10^0 width from 0^0 through 140^0 and a final interval of 140^0 to 180^0 . The final interval was made larger to have a reasonable number of entries. A unit vector in the equatorial coordinate system is constructed for each event. For each interval the vector difference between each event pair is calculated. These vectors are normalized to unity. If a given vector has a negative projection on the z-axis (north equatorial pole is positive) all three components are reversed in sign. For each interval a vector sum is made and the modulus of this resultant vector is computed. It is these 15 moduli that are compared to those expected from a isotropic distribution. This test attempts to reveal both scalar and vector deviations from isotropy. It was invented with no reference to the data and no attempt was made to optimize it.

We were eager to see the results of this quickly developed test. Hence we used Monte Carlo techniques to evaluate the isotropic probability. We generated an isotropic distribution by selecting randomly in right ascension and in declination. The declination was selected randomly from our observed declination distribution. A large number of simulations ($\sim 10^5$) was made for the event sample size (27 initially and 58 ultimately). The mean vector modulus for each interval was calculated. For each interval the absolute difference between the observed modulus and its mean expected for isotropy was divided by that mean. The sum of this quantity over the 15 intervals is the statistic used to establish the probability of isotropy. An example of the evaluation of the isotropic probability is shown in Figure 24 where for 10^5 trials of 58 events the isotropic selection produces a statistic which exceeds the data 184 times giving an isotropic probability of 1.8×10^{-3} as shown in Fig 18.

References

1. V. Hess, *Phys. Zeit.*, **13**, 1084, (1912).
2. D. Allard, *private communication* ; also K. Greisen, *Phys. Rev. Lett.*, **16**, 748, (1966); G.

- T. Zatsepin and V. A. Kuzmin, *Sov. Phys. JETP Lett. (Engl. Transl.)*, **4**, 78, (1966).
3. R. U. Abassi *et al.*, *Phys. Rev. Lett.*, **100**, 101101, (2008).
 4. M. Takeda *et al.*, *Astro. Part. Phys.*, **19**, 447 (2003).
 5. J. Abraham *et al.*, *Nucl. Instrum. Methods Phys. Res. A*, **523**, 50, (2004).
 6. M. Ave *et al.*, *Astropart. Phys.* **28**, 41, (2007).
 7. M. Nagano *et al.*, *Astropart. Phys.*, **22**, 235, (2004).
 8. G. W. Clark *et al.*, *Phys. Rev.*, **122**, 637, (1960).
 9. T. Yamamoto, Proc. 30th ICRC (2007), arXiv:0707.2638v1 [astro-ph] .
 10. J. Abraham *et al.*, *Phys. Rev.Lett.*, **101**, 061101, (2008).
 11. V. Olmos-Gilbaja, contribution to this conference, parallel session.
 12. J. Abraham *et al.*, *Science*, **318**, 188, (2007).
 13. M.-P. Véron-Cetty and P. Véron, *Astron. & Astrophys.* , **455**, 773, (2006).
 14. C. Bonafazi, contribution to this conference, parallel session.
 15. V. de Souza, contribution to this conference, parallel session.
 16. M. Settimo, contribution to this conference, parallel session: see also, J. Abraham *et al.*, *Astropart. Phys.*, **31**, 399, (2009); J. Abraham *et al.*, *Astropart. Phys.* , **29**, 188, (2008); J. Abraham *et al.*, *Astropart. Phys.*, **27**, 155, (2007).
 17. S. Navas, contribution to this conference, parallel session: see also J. Abraham *et al.*, *Phys. Rev.*, **D79**, 102001, (2009).
 18. J. de Melo Neto, Proc 31st ICRC (2009), arXiv:0906.2347[astro-ph].